Pure appl. geophys. 157 (2000) 1905–1928
0033–4553/00/121905–24 $ 1.50 + 0.20/0

Pure and Applied Geophysics

Numerical Simulation of Rock Failure and Earthquake Process on Mesoscopic Scale

YU-CANG WANG,[1] XIANG-CHU YIN,[1,2] FU-JIU KE,[1] MENG-FEN XIA[1] and KE-YIN PENG[2]

Abstract—On the basis of the lattice model of MORA and PLACE, Discrete Element Method, and Molecular Dynamics approach, another kind of numerical model is developed. The model consists of a 2-D set of particles linked by three kinds of interactions and arranged into triangular lattice. After the fracture criterion and rules of changes between linking states are given, the particle positions, velocities and accelerations at every time step are calculated using a finite-difference scheme, and the configuration of particles can be gained step by step. Using this model, realistic fracture simulations of brittle solid (especially under pressure) and simulation of earthquake dynamics are made.

Key words: Numerical simulation, discrete element method, lattice model, rock failure, earthquake process.

Introduction

Earthquake prediction still remains one of the most difficult problems, due to many reasons of which the poor understanding of the physical process of earthquakes is a major one. Essentially, an earthquake is a rapidly occurring fracture of the rocks in the interior of the earth (KNOPOFF, 1993) (intraplate earthquake), or is a slip instability controlled by friction (BRACE and BYERLEE, 1966) (an earthquake in plate boundaries). Either a damage theory to predict precisely the failure of such brittle solids is still in a very rudimentary stage, or full understanding of friction phenomenon has not come about, which may be the scientific reason for the difficulty of earthquake prediction.

Similarly, in seismology, it is still very difficult to study analytically the whole earthquake occurrence (spatial and temporal distribution of seismicity) with a large number of coupled fault systems in a geologically complex area.

[1] LNM, Institute of Mechanics, Chinese Academy of Sciences, Beijing, China, 100080.
[2] Center for Analysis and Prediction, China Seismological Bureau, Beijing, China, 100036. E-mail: WYC: yin@lnm.imech.ac.cn; YXC: yinxc@btamail.net.cn; KFJ: kefj@lnm.imech.ac.cn; XMF: xiam@lnm.imech.ac.cn; PKY: xcyin@public.bta.net.cn

In recent years, numerical simulation began to play a more important role in studying such complex phenomena. There are already many successful numerical models proposed to simulate earthquakes, such as the spring-block model (BURRIDGE and KNOPOFF, 1967; CARLSON and LANGER, 1989; CARLSON *et al.*, 1989), cellular automata (BARRIERE and TURCOTTE, 1991; LOMNITZ-ADLER, 1993; SAMMIS and SMITH, 1999), and SOC model (BÅK and TANG, 1989). These models only simulate the general aspects and statistical behaviors of the earthquake process.

Some simulations, such as finite element method (TANG, 1997), finite difference (DAY, 1982; MADARIAGA *et al.*, 1997), boundary integral equation method (FUKUYAMA and MADARIAGA, 1995) are based on the macroscopic and continuous media. But the earth's crust is far from being continuous, it contains many discontinuities of different sizes.

Molecular Dynamic simulation (MD, HERRMANN, 1989) provides a natural way to study the discrete behavior on a molecular/atomic scale, but when modeling earthquake phenomena, the scale must be many magnitudes coarser. It is difficult and unnecessary to model the earthquake process on a molecular/atomic scale. Discrete Element Method (DEM, CUNDALL and STRACK, 1979) is suitable to model the dynamic behavior of an assemblage of blocks and granular materials with discontinuities, and was widely used in engineering and geology.

Several kinds of discrete models have been used in mechanical and engineering fields to model failure and damage evolution of materials. Lattice models are commonly used. Central-force lattice or truss (ASHURT and HOOVER, 1976; CURTIN and SCHER, 1990a,b) is the simplest one, in which only axial forces can be transmitted. These models are simple and easy to handle. However, if the simulation is not on a molecular/atomic scale, negligence of transverse forces and moments may cause some problems, especially under compressive loads. On one hand, it may yield an unrealistic failure mode. On the other hand, if all link rigidity parameters are identical, Poisson's ratio is equal to 1/3, so central-force lattice has only one parameter, while an isotropic elastic solid is defined by two parameters. In the beam lattice (frame) (MONETTE and ANDERSON, 1994), bending rigidity is included to model forces due to the relative rotations of the links at nodes. In some lattice models (BORN and HUANG, 1954; ASKAR and CAKMAK, 1968; BATHURST and ROTHENBURG, 1988), axial and transverse forces can be transmitted.

Theoretically, there should be three kinds of relative displacements and therefore three kinds of interactions in order to make a perfect description of relative displacement between two adjacent particles. Therefore three kinds of rigidity parameters should be introduced. However, in order to make a realistic simulation, the three lattice parameters must match the two macroscopic elastic parameters and the failure criterion must be chosen carefully. Although a few researchers (JAGOTA and DAWSON, 1988a,b; JAGOTA and SCHERR, 1993; TOI and CHE, 1994; TOI and KIYOSUE, 1995) used models with three kinds of interactions transmitted, they did not describe how to determine the lattice parameters.

Lattice models have been applied to model earthquake phenomena. For example, MORA and PLACE (1993, 1994, 1998) developed a lattice called "the Lattice Solid Model (LSM)" to study earthquake dynamics whose initial version involved central forces, and used it to simulate the effect of fault gouge and surface roughness on friction and tried to explain the heat flow paradox. SCOTT (1996) modeled seismicity and stress rotation using the discrete lattice with central and shear forces transmitted.

On the basis of MORA and PLACE's LSM, DEM and Molecular Dynamic simulation, we studied another kind of discrete model. In this paper we describe our model first, then give the lattice parameters and some preliminary simulations on the fracture of brittle solid (especially under compressive loads) and the earthquake process.

About our Model

In our study, the material is also discretized into a number of round particles linked by bonds and arranged into a 2-D triangular lattice (Fig. 1). The particles are the smallest mesoscopic units which cannot be broken. The sizes of particles range from millimeter (grains) to kilometer (geological blocks). Radial forces F_r, tangential forces F_s and bending moment M are transmitted between the adjacent particles, and every particle is described by three variables: positions x, y and spin θ, so there are three kinds of relative displacements between every adjacent particle pair: radial displacement Δr, shear displacement Δs, and angular displacement $\Delta\theta$. If we use the linear relation of force and displacement, we have

$$\begin{aligned} F_r &= K_r\,\Delta r \\ F_s &= K_s\,\Delta s \\ M &= K_m\,\Delta\theta \end{aligned} \tag{1}$$

where K_r, K_s, K_m are radial, tangential and bending rigidity.

Elastic Properties and Chosen of Mesoscopic Parameters

We demonstrated (see appendix) that if K_r, K_s, K_m are identical, our model has isotropic elastic properties, and under the condition of small strain, the mesoscopic parameters K_r, K_s, K_m should be chosen according to the macroscopic Young modulus of elasticity E, and Poisson's ratio v,

$$K_r = \frac{\sqrt{3}E}{3(1-v)} \tag{2}$$

$$K_s = \alpha K_r \tag{3}$$

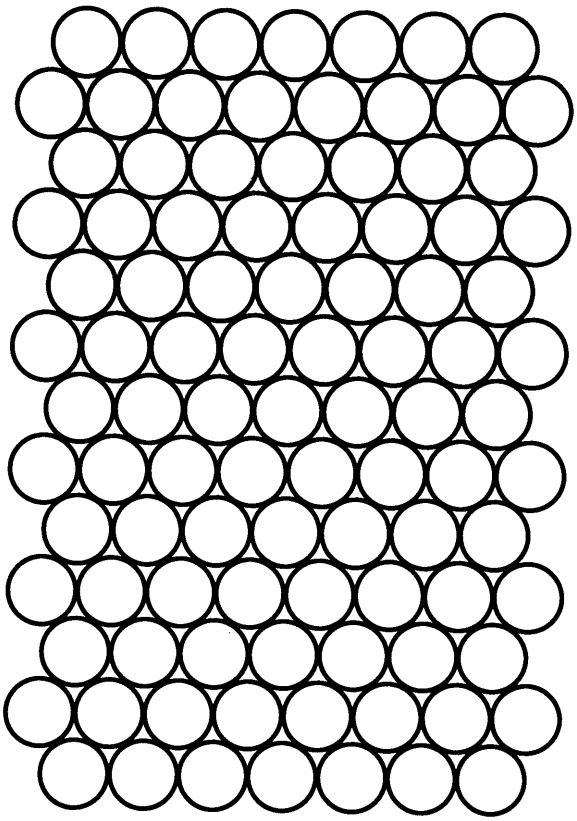

Figure 1
2-D Discrete lattice model.

$$K_m = \frac{\sqrt{3} r_0^2 E}{18} \tag{4}$$

where

$$\alpha = \frac{1 - 3v}{1 + v} \tag{5}$$

$$v = \frac{1 - \alpha}{3 + \alpha} \tag{6}$$

and r_0 is the diameter of the particles. The equations above reflect the connection between the mesoscopic and macroscopic parameters. From the equations above we also know that the materials of v from 0 to 1/3 can be modeled, and if the tangential rigidity is neglected ($K_s = 0$), $v = 1/3$.

Fracture Criterion and States after Fracture

The link between two adjacent particles can break independently in the following three different ways:
When radial extension force exceeds the maximum value F_{r0},
or, when tangential force exceeds the maximum value F_{s0},
or, when moment exceeds the maximum value M_0.

Generally three kinds of interactions always exist at the same time. We use the following empirical criterion similarly to judge if the link will break:

$$\frac{F_r}{F_{r0}} + \frac{|F_s|}{F_{s0}} + \frac{|M|}{M_0} \geq 1. \tag{7}$$

In the simulation, we choose $F_{r0} = K_r(\Delta r)_m = K_r r_0 \varepsilon_m$, $\varepsilon_m = 0.005$–0.010, $F_{s0} = CF_{r0}$ and $M_0 = Dr_0F_{r0}$, where $C = 0.3$–0.7 and $D = 1/6$ are chosen empirically. The effect of radial force on the tangential and bending fracture is considered.

There are four kinds of linking states between neighboring particles:
(A) Intact, (B) Sliding, (C) Locked by static friction, (D) Departing.
Table 1 shows whether or not the forces and moment can be transmitted in each case.

The states can change according to:
(a) A → B, when (7) is met, and $r \leq r_0$ and $V_t \neq 0$
(b) A → D, when (7) is met, and $r \geq r_0$
(c) B → C, when $V_t = 0$
(d) C → B, when $f_s \geq \mu_s F_r$
(e) B → D, when $r \geq r_0$
(f) C → D, when $r \geq r_0$
(g) D → B, when $r \leq r_0$ and $V_t \neq 0$
(h) D → C, when $r \leq r_0$ and $V_t = 0$
where f_s stands for static frictional force, μ_s refers to static frictional coefficient, and V_t, is relative tangential velocity.

Table 1

f_d and μ_d are sliding frictional force and sliding frictional coefficient, respectively.

	F_r	F_s	M
A	can	can	can
B	can, only when $r \leq r_0$	sliding frictional force $f_d = \mu_d F_r$	cannot
C	can, only when $r \leq r_0$	static frictional force	cannot
D	cannot	cannot	cannot

Calculation of Static Friction

When two particles are locked by static friction, if the tangential rigidity is chosen to be infinite (PLACE and MORA, 1999), the frictional forces are calculated according to all forces acting on the particles. This is a difficult step considering that frictional forces are all inter-dependent when infinite shear rigidity is chosen. In our model, the tangential rigidity is not infinite, but a finite one. The static frictional force can be easily decided by the relative tangential displacement according to the principle of DEM. Figure 2 illustrates how the shear forces between bonded particles are calculated. Similarly, static frictional forces are calculated from the relative displacements at the contact surfaces (cf., Fig. 3).

Solution of Equation of Motion

The differential scheme of MD is used as in MORA's model, with the only difference of adding the equation of θ. Due to the changes of linking states between two adjacent particles (e.g., breaking and sliding), the forces and accelerations may be discontinuous. These discontinuities are dealt with from $t^- + \Delta t$ to $t^+ + \Delta t$, and no breaking and sliding occurs from t^+ to $t^- + \Delta t$. However, the positions and velocities are continuous. These quantities are calculated in the following way.

First, calculate the positions at $t + \Delta t$

$$\begin{cases} \vec{X}_i(t+\Delta t) = \vec{X}_i(t) + \Delta t\, \vec{X}'_i(t) + \dfrac{(\Delta t)^2}{2}\, \vec{X}''_i(t^+) \\ \theta_i(t+\Delta t) = \theta_i(t) + \Delta t\, \theta'_i(t) + \dfrac{(\Delta t)^2}{2}\, \theta''_i(t^+) \end{cases} . \tag{8}$$

Second, calculate the forces (and moments) and accelerations at $t^- + \Delta t$,

$$\begin{cases} \vec{X}''_i(t^- + \Delta t) = \vec{F}_i(t^- + \Delta t)/m_i \\ \theta''_i(t^- + \Delta t) = M_i(t^- + \Delta t)/I_i \end{cases} \tag{9}$$

where m_i and I_i are the mass and rotational inertia of the i-th particle. Then we calculate the velocities at $t + \Delta t$

$$\begin{cases} \vec{X}'_i(t+\Delta t) = \vec{X}'_i(t) + \dfrac{\Delta t}{2}\left[\vec{X}''_i(t^+) + \vec{X}''_i(t^- + \Delta t)\right] \\ \theta'_i(t+\Delta t) = \theta'_i(t) + \dfrac{\Delta t}{2}\left[\theta''_i(t^+) + \theta''_i(t^- + \Delta t)\right] \end{cases} . \tag{10}$$

Finally, judge whether breaking or sliding occurs between any particles pair, if so, update the forces and accelerations from $t^- + \Delta t$ to $t^+ + \Delta t$ according to the rules mentioned above.

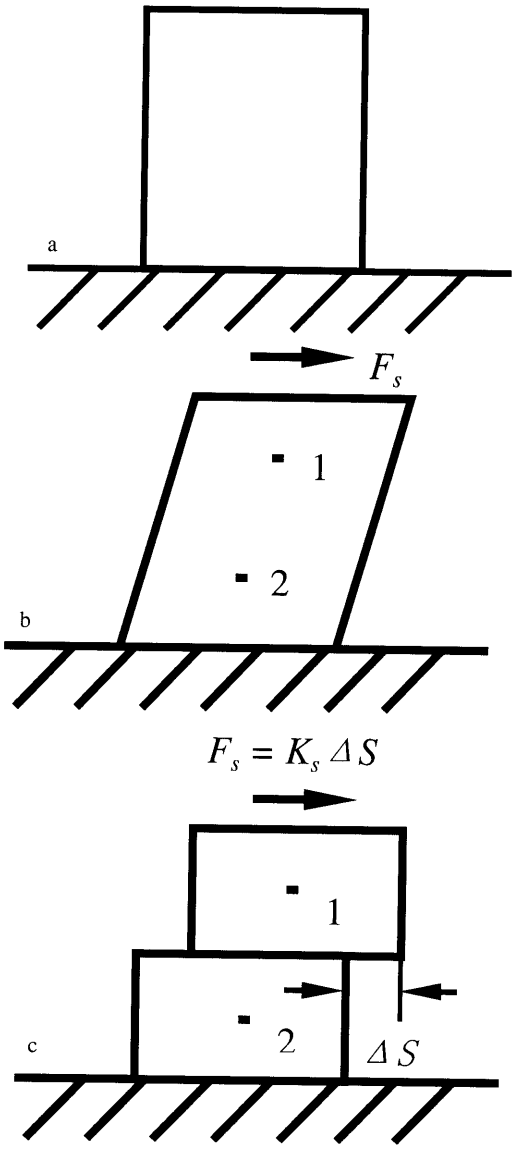

Figure 2
Sketch of calculation of shear forces using the Discrete Element Method in which a sample is subjected to shear load. The initial sample (inset a), composed of two bonded blocks, is subjected to a shear force (inset b). By assuming that the blocks are rigid, the resulting shear force between block 1 and block 2 can be calculated from the relative displacement of the blocks (inset c).

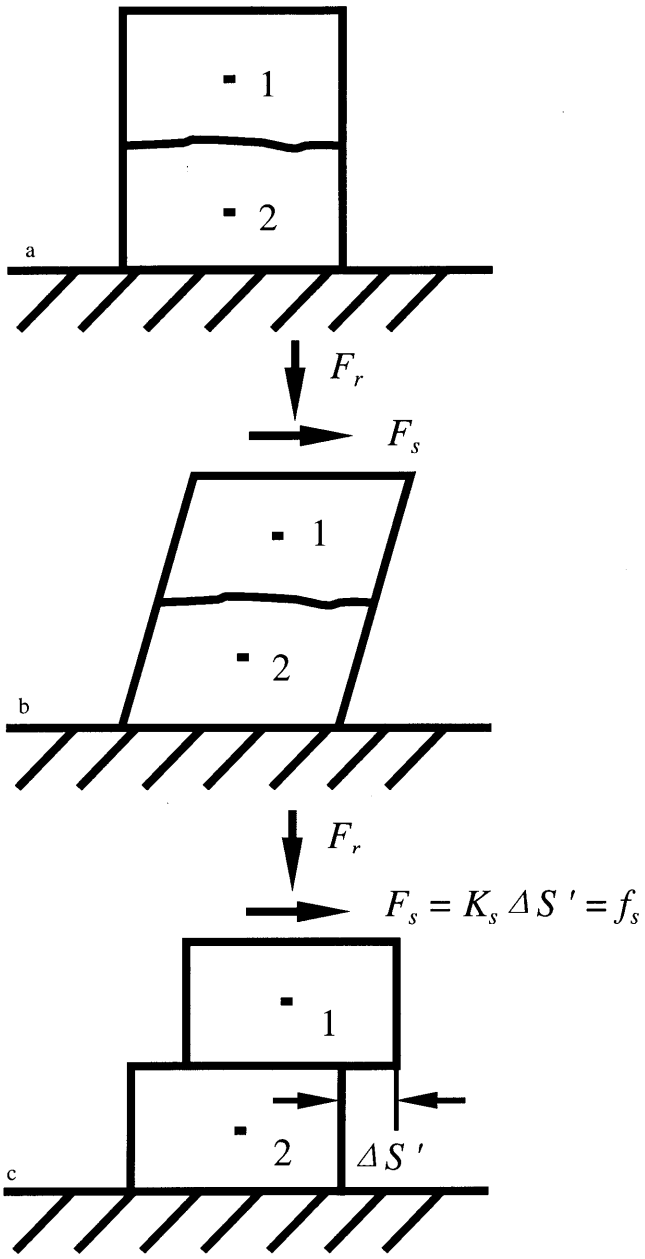

Figure 3
Sketch of calculation of static frictional force. The initial sample (inset a) is composed of two unbonded blocks locked by static friction. When subjecting the sample to a shear force, shear deformations occur (inset b). By assuming that the blocks are rigid, the frictional forces locking the two blocks can be calculated from the relative displacement of the two blocks (inset c).

Viscosity is also introduced, so $\vec{F}_i = \vec{F}_i^{\mathrm{I}} + \vec{F}_i^{\eta}$, $\vec{F}_i^{\mathrm{I}}$ includes elastic forces and frictional forces, $\vec{F}_i^{\eta}$ is viscous force. We use

$$\vec{F}_{ij}^{\eta} = -\eta(\bar{V}_i - \bar{V}_j) \tag{11}$$

where η is coefficient of viscosity. Equations (9), (10) and (11) indicate that due to the viscosity, computation of the accelerations at $t^- + \Delta t$ requires the velocities at $t + \Delta t$, however the velocities update also requires accelerations at $t^- + \Delta t$, so iteration must be used to calculate $\vec{X}_i'(t + \Delta t)$.

First, we choose a group of approximate trial solutions $\tilde{\vec{X}}_i'(t + \Delta t)$

$$\tilde{\vec{X}}_i'(t + \Delta t) = \vec{X}_i'(t) + \Delta t \vec{X}_i''(t) \quad (i = 1, N)$$

then use the following iteration scheme. (take $\tilde{x}_i'(t + \Delta t)$ as an example),

$$\begin{cases} \text{Calculate } \vec{F}_i^{\eta} \text{ (Eq. 11)} \\ \text{Calculate } \vec{F}_i(t^- + \Delta t) \text{ and } x_i''(t^- + \Delta t) \text{ (Eq. 8) (Eq. 9)} \\ \text{Calculate } x_i'(t + \Delta t) \text{ (Eq. 10)} \\ \text{Compare } \tilde{x}_i'(t + \Delta t) \text{ with } x_i'(t + \Delta t): \\ \text{If } \left| \dfrac{\tilde{x}_i'(t + \Delta t) - x_i'(t + \Delta t)}{x_i'(t + \Delta t)} \right| \geq \varepsilon \text{ then} \\ \tilde{x}_i'(t + \Delta t) = \tilde{x}_i'(t + \Delta t) \text{ and repeat iteration} \\ \text{If } \left| \dfrac{\tilde{x}_i'(t + \Delta t) - x_i'(t + \Delta t)}{x_i'(t + \Delta t)} \right| \leq \varepsilon \text{ then} \\ \tilde{x}_i'(t + \Delta t) = \tilde{x}_i'(t + \Delta t) \text{ and stop iteration} \end{cases}$$

where ε stands for an iteration precision. The convergence rate is rapid and three to four iterations were adequate.

Some Preliminary Results

Uniaxial Compressive Test

The failure process of brittle rocks under compressive stress was modeled. In our numerical test, the number of particle is 25×51, $m = 1.0$, $r_0 = 4.0$, $K_r = 1000$, $dt = 0.01$, $v = 0.2$, $\eta = 0.6$. K_s, K_m and E are decided according to equations (2)–(6). Figure 4 shows the results of a homogeneous, intact sample subjected to increased uniaxial compressive stress on the top and bottom ($\sigma = 0.2\ t$). The black lines mean that the links between two particles are intact, the grey ones stand for broken but

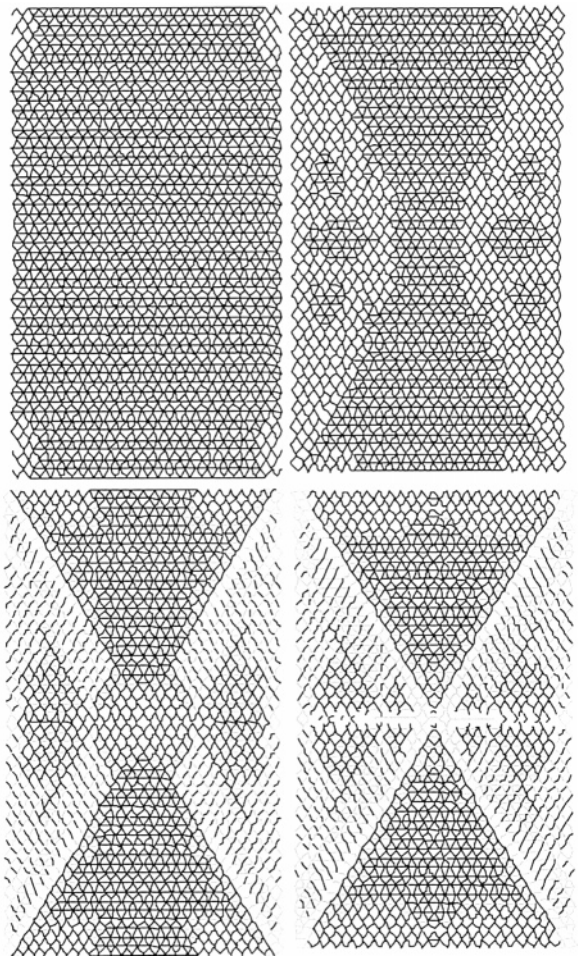

Figure 4
The fracture process of a homogeneous sample (all of the rigidity parameters and fracture parameters are identical) subjected to uniaxial compressive load.

contacting links, and disappearances of lines represent broken links. First, extensive cracks ($r \geq r_0$ when broken) appear on the corners, then spread inside. Later, shear cracks ($r < r_0$ when broken) spread along the diagonals, forming macroscopic conjugate X-shaped failure patterns with two relative intact pyramidal parts and two relative fractured parts.

If disorder is introduced, the results may be different. For example, Figure 5 shows the sample with 2% randomly distributed initial defects. By defects, we mean the bonds are pre-broken but the adjacent particles are still in contact with one

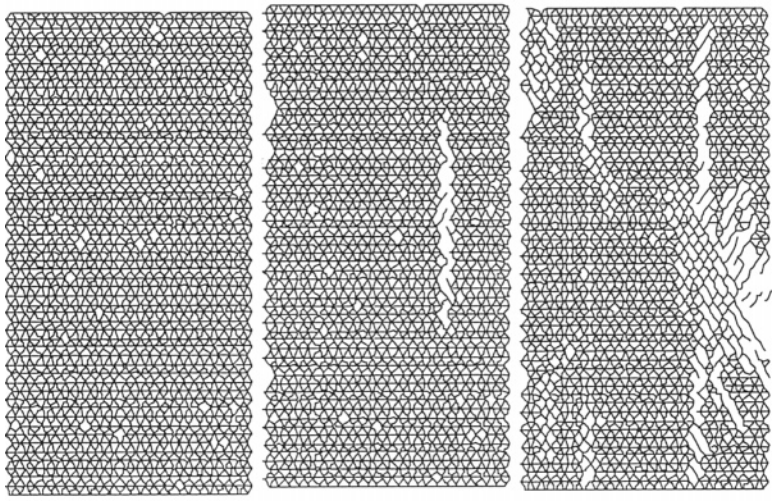

Figure 5
Brittle cleavage of material sample subjected to uniaxial compressive load, 2% bonds are randomly broken before loading.

another. In this case, vertical cleavage appears abruptly, then follows collapse of the sample, which is often observed in brittle rock experiments.

In addition, the dynamic expansion of closed oblique crack is also simulated (Fig. 6). It is seen that tensile cracks expand from the tips of the oblique crack. The results are also similar with rock experiments (BRACE, 1960; BRACE and BOMBALAKIS, 1963).

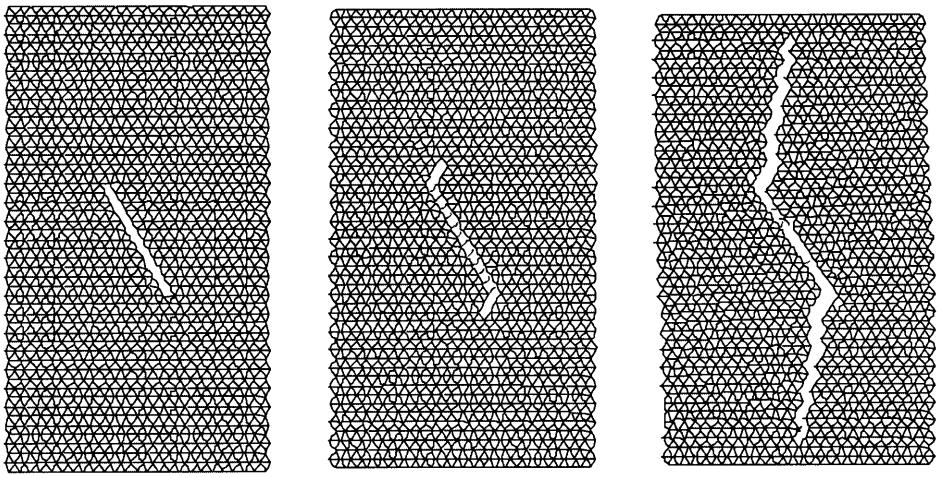

Figure 6
Extension of closed oblique crack under uniaxial pressure, tensile cracks ($r \geq r_0$ when broken) expand from the tips of the oblique crack.

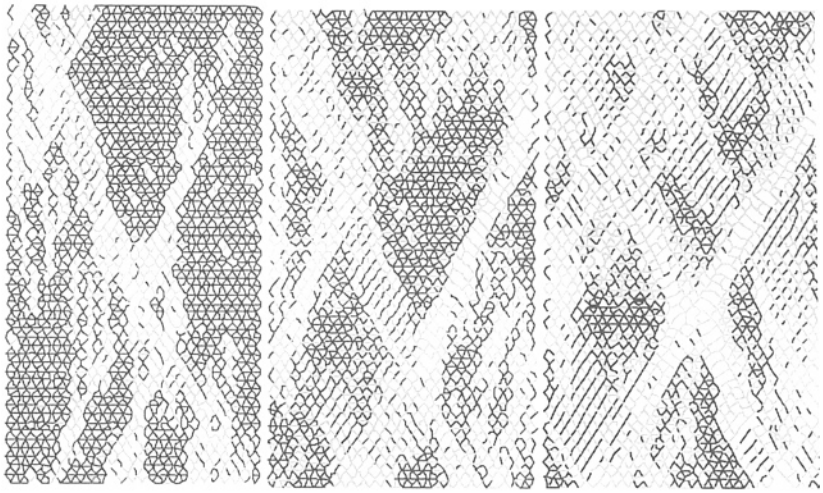

Figure 7
Effects of confining pressure on macroscopic failure modes. Axial stress $\sigma_1 = 0.2t$, confining pressure $\sigma_2 = \lambda\sigma_1$ for $t < 10$ and $\sigma_2 = \text{const}$ for $t > 10$. From left to right, $\lambda = 0.1$, 0.2, 0.4, confining pressure is increasing, the angles between two groups of shear bands are increasing, and more shear bands can be seen.

Effects of Confining Pressure

If there is confining pressure, the failure pattern is represented by two groups of shear bands nearly along two diagonal directions. The effect of confining pressure on failure patterns is obvious in Figures 7 and 8, with an increase of the confining pressure, the failure process tends to be more ductile; the strength becomes larger; there are more shear bands in each group, and the angle between two groups of main shear bands also increases.

Simulation of Seismicity

Considering that earthquakes in China are mainly intraplate earthquakes, we used a model different from the earthquake model for transform faults (such as the San Andreas Fault). In this model (Fig. 9) faults of different sizes are distributed in random directions and positions; the model is subjected to an increased compressive load and confining pressure. An earthquake is defined as an event releasing potential energy, such as the breaking of a single bond or sliding between two particles, but if the adjacent events occur in successive time steps, these are considered to be part of a single larger event. The magnitudes are decided according to the potential energy E released by the broken bonds

$$M = c_1 + c_2 \log E \tag{12}$$

where c_1 and c_2 are constants. In seismology, $\log E = 11.8 + 1.5\ M$, so $c_1 = -7.8667$, $c_2 = 0.6667$. Here we still choose $c_2 = 0.6667$, c_1 is chosen to make the magnitude of the smallest event be 0. In this way, seismic activity, such as frequency (Fig. 10), energy release (Fig. 11) and M-t charts (Fig. 12) are gained using this model.

Some factors that influence b values are discussed. The random precracks are distributed according to $P(l) \propto cl^{-\gamma}$, where c is a constant, representing the density of cracks, l is the length of faults (SCHOLZ and COWIE, 1990), and $\gamma > 0$. b values are calculated according to the well-known G-R relation. In Figure 13 it is easy to see that the more cracks there are (the bigger c is), the bigger the b values are,

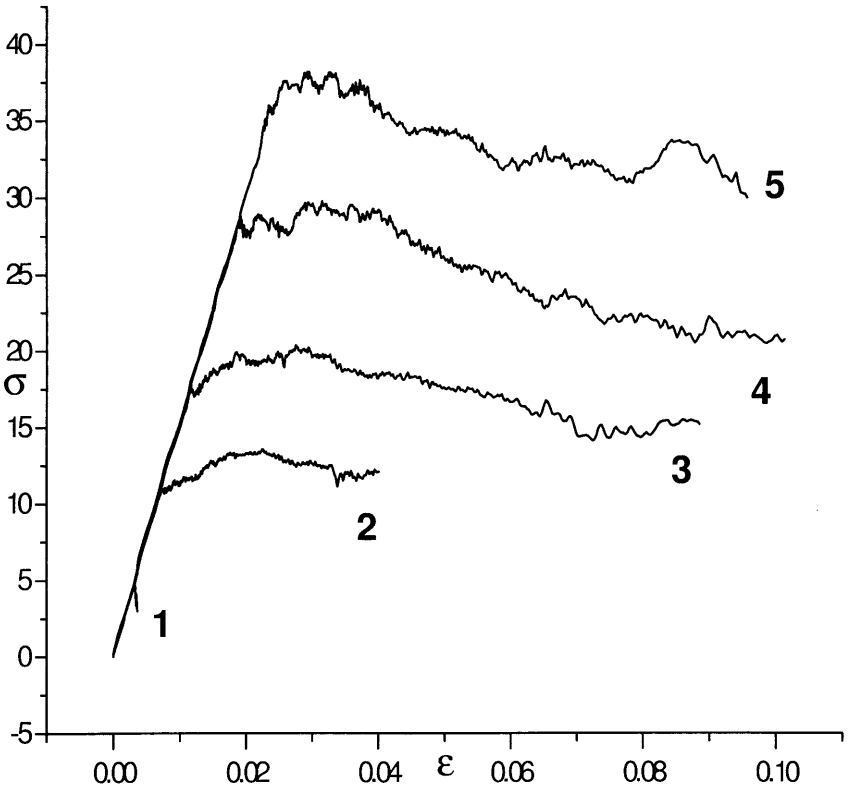

Figure 8
The simulated axial stress-strain curves with different confining pressure. Curve 1 has no confining pressure ($\lambda = 0$), brittle fracture is seen, from 2 to 5, $\lambda = 0.1$, 0.2, 0.4, 0.6. With the increase of confining pressures, the strengths also increase. The fracture processes tend to be more ductile.

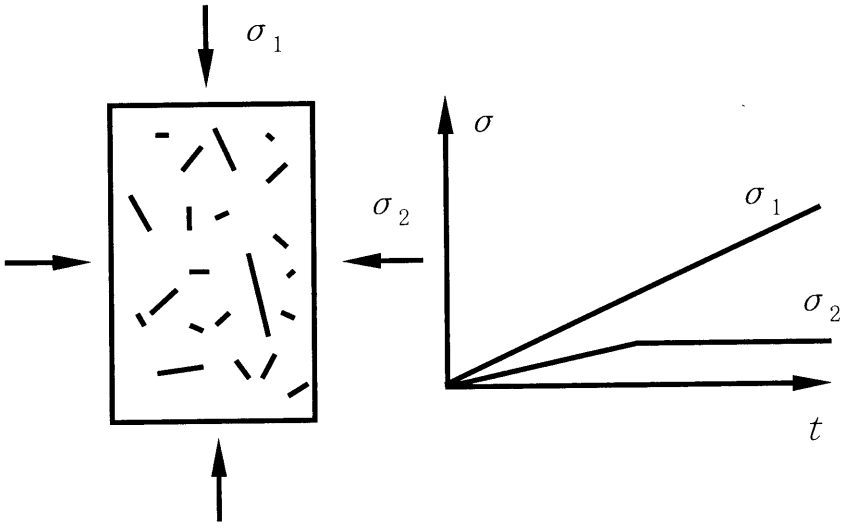

Figure 9
An earthquake model with random cracks. The model is subjected to increased compressive load $\sigma_1 = 0.2\ t$ and confining pressure which increases first and then remains constant ($\sigma_2 = 0.2\sigma_1$ for $t < 10$ and $\sigma_2 = \text{const}$ for $t > 10$).

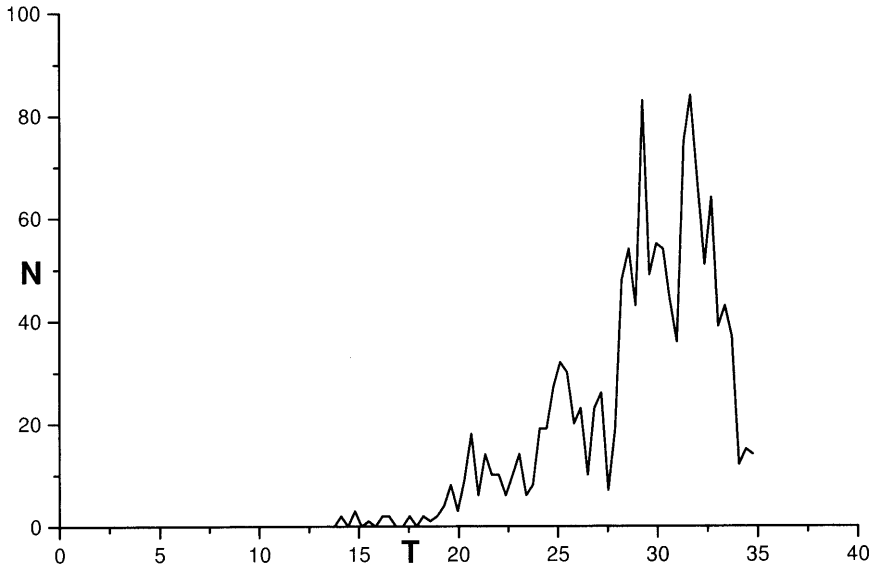

Figure 10
The variations of frequency (numbers of earthquakes during per unit time) of modeled earthquakes with time.

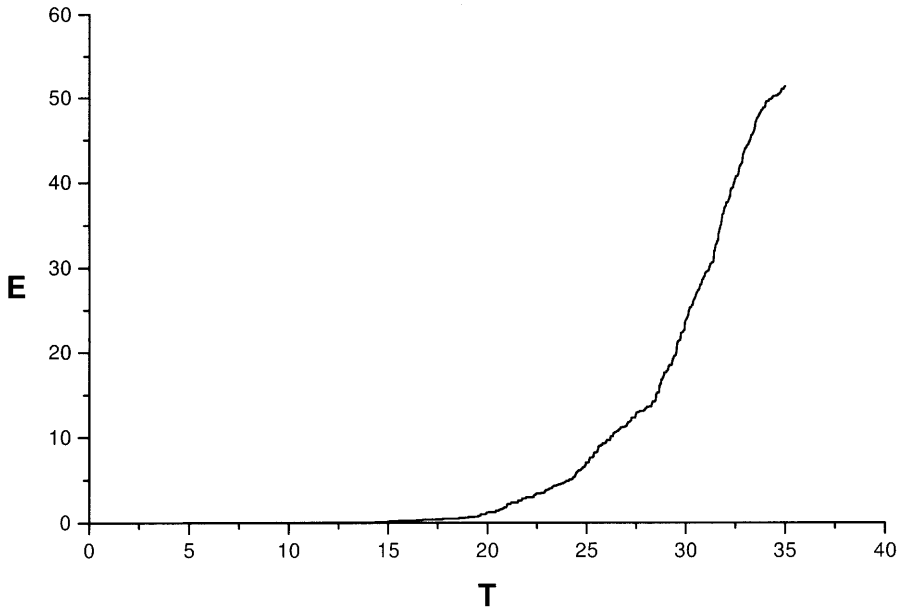

Figure 11
Plot of accumulated energy released by breaking of bonds or sliding between particle pairs, accelerated releases of energy correspond to bigger earthquakes.

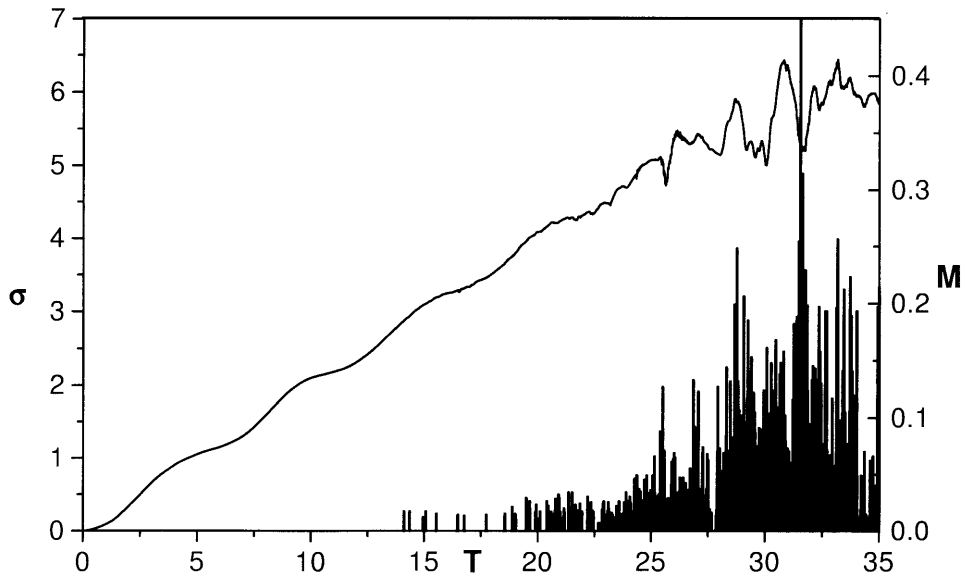

Figure 12
Modeled magnitudes of events and main compressive stress curves. The stress drops correspond to earthquakes.

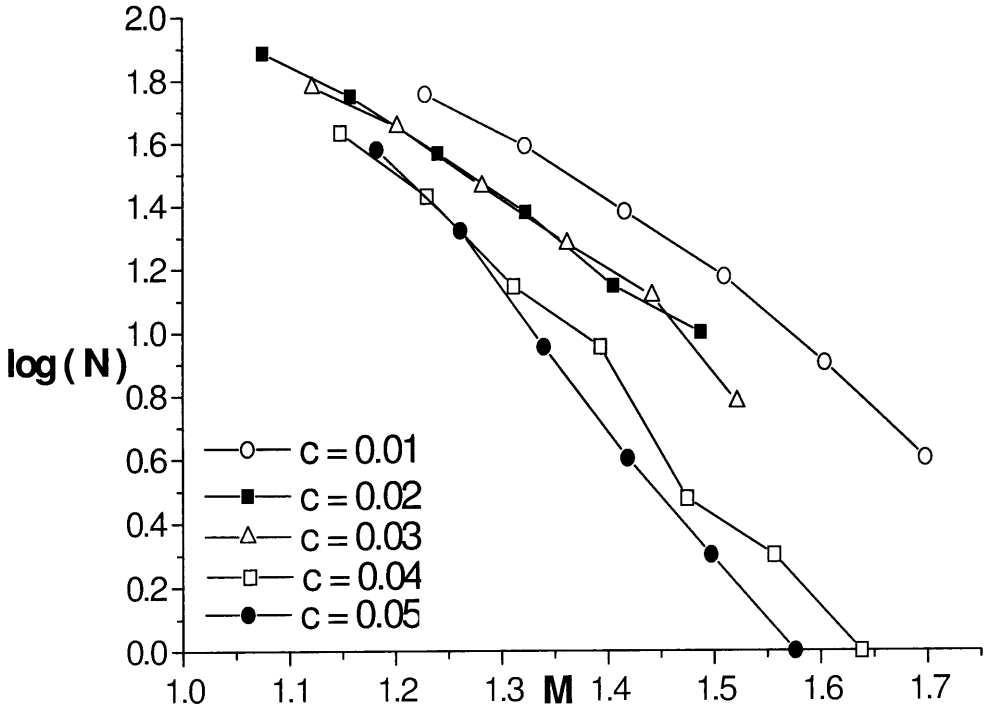

Figure 13
The effect of crack density on b values, with increasing of crack density c, b values (the slope of $\log N - M$ relation) increase.

which is similar to the results of MOGI (1976). In Figure 14 γ is also an important effecting factor. The bigger γ is (which means that there are more short faults and less long faults), the bigger the b values are. In fact, besides the density of faults and length distribution, there must be other effecting factors, such as inhomogeneous distribution of strength and elastic constants, which deserves further study.

Numerical Study of Load/Unload Response Ratio Theory

Tidal forces generated by the moon and the sun exert periodic loads and unloads on the earth's crust. When the focal region is in a stable state, the responses to this loading and unloading are approximately equal, however when the focal region is unstable and near fracture, the responses are quite different. According to this principal, YIN proposed Load/Unload Response Ratio Theory (LURR, YIN *et*

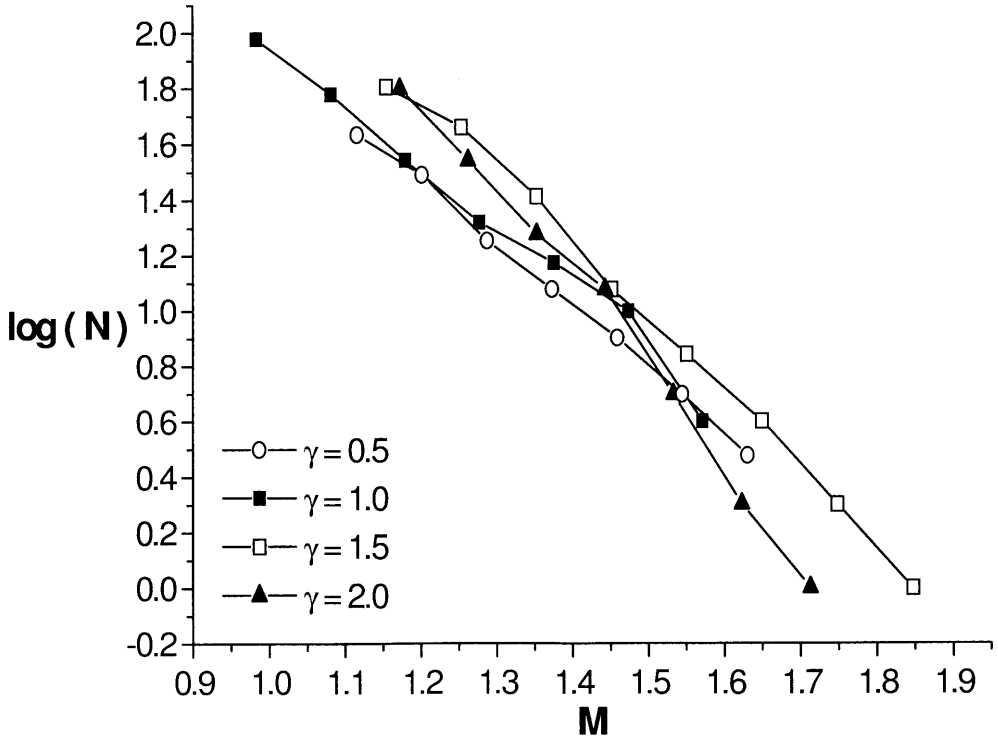

Figure 14
The effect of distribution of length of cracks on b values, with increasing γ (there are more short cracks and less long ones), b values increase.

al., 1995) to judge the imminence of earthquake. This method is successfully applied for medium-term earthquake prediction (YIN *et al*., 2000, this issue).

We simulated LURR theory using the model above. The main compressive stress is increased with a small additional sine-shaped disturbance, which modeled loading and unloading. LURR values are decided by

$$\mathrm{LURR} = \frac{\sum \sqrt{E_+}}{\sum \sqrt{E_-}} \tag{13}$$

where E_+ and E_- are earthquake energy released during loading and unloading periods, respectively. Figure 15 presents the results. Figure 16 is an M-t chart corresponding to Figure 15. It is clearly seen that LURR values fluctuate about

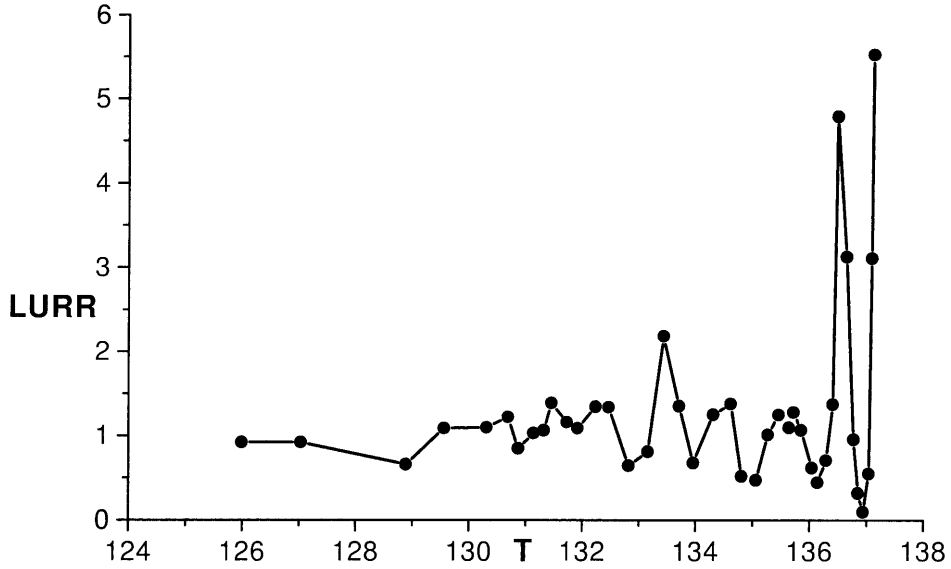

Figure 15
Simulated variations of Load/Unload Response Ratio (LURR) with time, LURR values fluctuate about 1 when there is no large earthquake or when seismicity is weak, before the largest earthquake ($T = 137.05$), LURR values rise markedly.

1 when there is no large earthquake or when the seismicity is low, but before the largest earthquake in the sequence, LURR values rise markedly, which is similar to real earthquake cases (YIN *et al.*, 2000, this issue). This indicates that LURR is a quantitative parameter to judge the closeness of an earthquake.

Conclusion

The preliminary simulations indicate that the model is capable of simulating rock failure, especially under compressive loads. However when modeling the earthquake process, our simulations are still coarse, since the number of particles is very small. Simulations have a narrow range of grain sizes, whereas grain sizes in the crust have a broad distribution, therefore large scales of simulations are needed in future work.

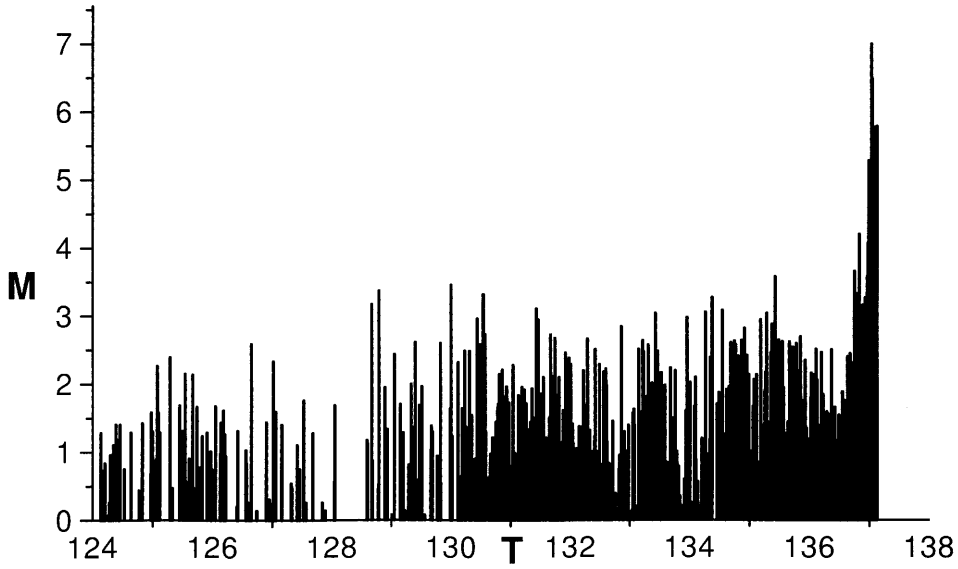

Figure 16
M-t chart corresponding to Figure 15.

Acknowledgements

This research was funded by the National Scientific Foundation of China (Grant No. 19732060), the Earthquake Association Foundation (Grant No. 95-07-435), and the Laboratory of Nonlinear Mechanics, Institute of Mechanics, CAS. The authors are grateful to Prof. MORA and Dr. PLACE for their valued suggestions.

Appendix

In order to make a realistic simulation, the lattice rigidity parameters K_r, K_s, K_m cannot be chosen arbitrarily, but must be chosen according to the elastic parameters of the continuum E and v. We determine these parameters by letting the nodal displacements of the lattice equal the displacements of corresponding points in the continuum subjected to specifically chosen strain conditions (so-called patch test, BATHE and WILSON, 1976).

First, consider the case of uniaxial elongation (Fig. 17). The stresses, strains and displacements (u, v) are

$$\begin{cases} \sigma_x = 2q \\ \sigma_y = 0 \\ \tau = 0 \end{cases}, \quad \begin{cases} \varepsilon_x = \dfrac{2q}{E} \\ \varepsilon_y = -\dfrac{2qv}{E} \\ \gamma = 0 \end{cases} \quad \text{and} \quad \begin{cases} u = \dfrac{2q}{E}\, x \\ v = -\dfrac{2qv}{E}\, y \end{cases}$$

and the strain energy density is $\phi = 2q^2/E$, where q is a small value such that $\varepsilon_x = 2q/E \ll 1$, the radial elongation between particles A and B is

$$\Delta r_{AB} = \int \varepsilon_{AB}\, dl_{AB} = \frac{q}{2E}(3 - v) r_0$$

where ε_{AB} is extension strain in AB direction, r_0 equilibrium distance between two adjacent particles.

$$\Delta r_{AC} = \frac{q}{2E}(3 - v) r_0$$

$$\Delta s_{AB} = \Delta s_{AC} = \frac{\sqrt{3} q}{2E}(1 + v) r_0$$

$$\Delta r_{BC} = \frac{2q}{E} v r_0$$

$$\Delta s_{BC} = 0$$

where Δs_{AB} represents transverse displacement between particles A and B. The potential energy stored in triangle ABC

$$E_p = \tfrac{1}{2}[\tfrac{1}{2} K_r(\Delta r_{AB}^2 + \Delta r_{AC}^2 + \Delta r_{BC}^2) + \tfrac{1}{2} K_s(\Delta s_{AB}^2 + \Delta s_{AC}^2 + \Delta s_{BC}^2)] = \tfrac{1}{2} r_0 \frac{\sqrt{3} r_0}{2} \phi,$$

$$K_r(3v^2 - 2v + 3) + K_s(v^2 + 2v + 1) = \frac{4\sqrt{3}}{3} E. \tag{14}$$

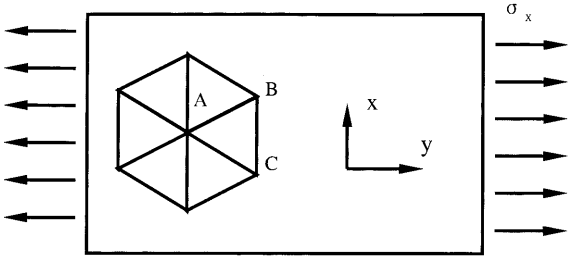

Figure 17
The lattice and continuum model subjected to uniaxial tensile stress. The nodal displacements of the lattice equal the displacements of corresponding points in the continuum, subjected to some specifically chosen strain conditions. Lattice parameters can be decided such that the lattice has realistic elastic properties.

In the second case (Fig. 18), the stresses become

$$\begin{cases} \sigma_x = 0 \\ \sigma_y = 0 \\ \tau = -p \end{cases}$$

where p is a small value such that $p/E \ll 1$. Similarly, we have

$$K_r + K_s = \frac{2\sqrt{3}}{3} \frac{E}{1+v}. \tag{15}$$

From (13) and (14), K_r and K_s can be solved

$$K_r = \frac{\sqrt{3}E}{3(1-v)} \tag{16}$$

$$K_s = \frac{1-3v}{1+v} K_r. \tag{17}$$

In both cases above, the rigid rotation $\omega_z = \frac{1}{2}(\partial v/\partial x - \partial u/\partial y) = 0$, $\Delta\theta = 0$, so K_m is not involved.

In the third case (Fig. 19), the object is subjected to a bending moment:

$$\begin{cases} \sigma_x = 6hy \\ \sigma_y = 0 \\ \tau = 0 \end{cases} \quad \text{and} \quad \begin{cases} \varepsilon_x = \dfrac{6h}{E} y \\ \varepsilon_y = -\dfrac{6hv}{E} y \\ \gamma = 0 \end{cases}$$

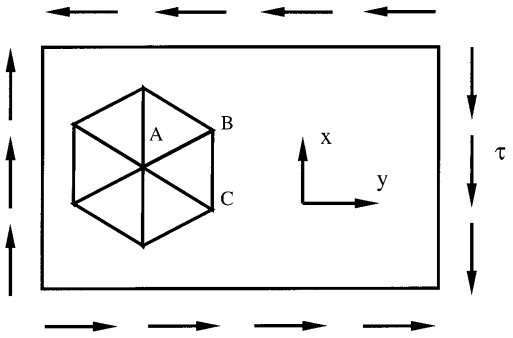

Figure 18
The lattice and continuum model subjected to shear stress.

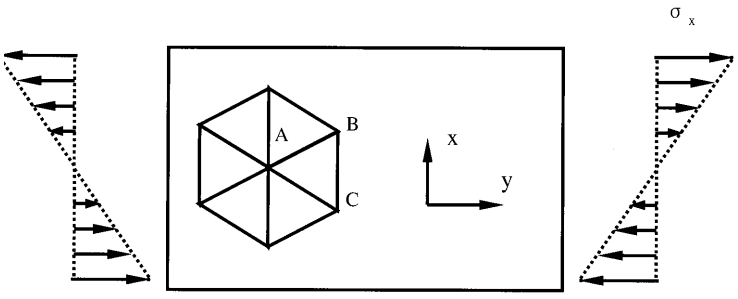

Figure 19
The lattice and continuum model subjected to bending moment.

where h is a small constant such that $h/E \ll 1$. In this case, the strain energy density is

$$\phi = \frac{18h^2}{E} y^2$$

and the rigid rotation is $\omega_z = -6hx/E$, K_m is involved in, and the energy caused by the bending between two particles must be taken into account. Similarly, we can obtain

$$K_m = \frac{\sqrt{3} r_0^2 E}{18}. \tag{18}$$

Lastly, if the lattices in Figures 17–19 are turned over an arbitrary angle a, the parameter a does not appear in equations (14)–(18). Hence, such a lattice is isotropic if K_r, K_s, K_m are identical for all particle pairs.

References

Ashurt, W. T., and Hoover, W. G. (1976), *Microscopic Fracture Studies in the Two-dimensional Triangular Lattice*, Phys. Rev. B *14*, 1465–1473.

Askar, A., and Cakmak, A. S. (1968), *A Structural Model of a Micropolar Continuum*, Int. J. Eng. Sci. *6*, 583–589.

Bäk, P., and Tang, C. (1989), *Earthquakes as a Self-organized Critical Phenomena*, J. Geophys. Rev. *94*, 15,635–15,637.

Barriere, B., and Turcotte, D. L. (1991), *A Scale—Invariant Cellular—Automata Model for Distributed Seismicity*, Geophys. Res. Lett. *18*, 2011–2014.

Bathe, K. J., and Wilson, E. L., *Numerical Methods in Finite Element Analysis* (Prentice-Hall, Inc. Englewood Cliffs, NJ 1976).

Bathurst, R. J., and Rothenburg, L. (1988), *Micromechanical Aspects of Isotropic Granular Assemblies with Linear Contact Interactions*, J. Appl. Mech. *55*, 17–23.

BORN, M., and HUANG, K., *Dynamical Theory of Crystal Lattice* (Oxford Univ. Press, New York, NY 1954).

BRACE, W. F. (1960), *An Extension of the Griffith Theory of Fracture to Rocks*, J. Geophys. Rev. *65*, 3477–3480.

BRACE, W. F., and BOMBALAKIS, E. G. (1963), *A Note on Brittle Crack Growth in Compression*, J. Geophys. Rev. *68*, 3709–3713.

BRACE, W. F., and BYERLEE, J. D. (1966), *Stick-slip as a Mechanism for Earthquakes*, Science *153*, 990–992.

BURRIDGE, R., and KNOPOFF, L. (1967), *Model and Theoretical Seismicity*, B.S.S.A. *57*, 341–371.

CARLSON, J. M., and LANGER, J. S. (1989), *Mechanical Model of an Earthquake Faults*, Phys. Rev. A *40*, 6470–6484.

CARLSON, J. M., LANGER, J. S., and SHAW, B. E. (1989), *Dynamics of Earthquake Faults*, Rev. Mod. Phys. *66*, 657–670.

CUNDALL, P. A., and STRACK, O. D. L. (1979), *A Discrete Element Model for Granular Assemblies*, Geotechnique *29*, 47–65.

CURTIN, W. A., and SCHER, H. (1990a), *Brittle Fracture in Disordered Materials: A Spring Network Model*, J. Mater. Res. *5*, 535–553.

CURTIN, W. A., and SCHER, H. (1990b), *Mechanics Modeling Using a Spring Network*, J. Mater. Res. *5*, 554–562.

DAY, S. M. (1982), *Three-dimensional Finite Difference Simulation of Faults Dynamics: Rectangular Faults with Fixed Rupture Velocity*, B.S.S.A. *72*, 705–727.

FUKUYAMA, E., and MADARIAGA, R. (1995), *Integral Equation Method for Plane Crack with Arbitrary Shape in 3-D Elastic Medium*, B.S.S.A. *85*, 614–628.

HERRMANN, D. W., *Computer Simulation Methods in Theoretical Physics*, second edition (Springer-Verlag, Berlin, New York 1989).

JAGOTA, A., and DAWSON, P. R. (1988a), *Micromechanical Modeling of Powder Compacts—I. Unit Problems for Sintering and Traction Induced Deformation*, Acta Metall. *36*, N,2551–2561.

JAGOTA, A., and DAWSON, P. R. (1988b), *Micromechanical Modeling of Powder Compacts—II. Truss Formulation of Discrete Packing*, Acta Metall. *36*, 2563–2573.

JAGOTA, A., and SCHERR, G. W. (1993), *Viscosities and Sintering Rates of a Two-dimensional Granular Composite*, J. Am. Ceram. Soc. *76*, 3123–3135.

KNOPOFF, L. (1993), *Self-organization and the Development of Pattern: Implications for Earthquake Prediction*, Proceedings of the American Philosophical Society *137*, 3.

LOMNITZ-ADLER, J. (1993), *Automation Models of Seismic Fracture: Constraints Imposed by Magnitude-frequency Relation*, J. Geophys. Rev. *98*, 17,745–17,756.

MADARIAGA, R., OLSEN, K. B., and ARCHULETA, R. J. (1997), *3-D Finite-difference Simulation of a Spontaneous Rupture*, Seismol. Res. Lett. *68*, 312.

MOGI, K. (1976), *Regional Variations in Magnitude Frequency Relation of Earthquakes*, Bull. Earthquake Res. Inst. *45*, 313–325.

MONETTE, L., and ANDERSON, M. P. (1994), *Elastic and Fracture Properties of the Two-dimensional Triangular and Square Lattice*, Modelling Simul. Mater. Sci. Eng. *2*, 52–66.

MORA, P., and PLACE, D. (1993), *A Lattice Solid Model for the Nonlinear Dynamics of Earthquakes*, Int. J. Mod. Phys. C *4*, 1059–1074.

MORA, P., and PLACE, D. (1994), *Simulation of the Frictional Stick-slip Instability*, Pure appl. geophys. *143*, 61–87.

MORA, P., and PLACE, D. (1998), *Numerical Simulation of Earthquake Faults with Gouge: Towards a Comprehensive Explanation for the Heat Flow Paradox*, J. Geophys. Res. *103*, 21,067–21,089.

PLACE, D., and MORA, P. (1999), *The Lattice Solid Model to Simulate the Physics of Rocks and Earthquake: Incorporation of Friction*, J. Comp. Phy. *150*, 332–372.

SAMMIS, C. G., and SMITH, S. W. (1999), *Seismic Cycles and the Evolution of Stress Correlation in Cellular Automation Models of Finite Faults Networks*, Pure appl. geophys. *155*, 307–334.

SCOTT, D. R. (1996), *Seismicity and Stress Rotation in a Granular Model of the Brittle Crust*, Nature *381*, 592–595.

SCHOLZ, C. H., and COWIE, P. A. (1990), *Determination of Geologic Strain from Fault Slip Data*, Nature *346*, 837–839.

TANG, C. A. (1997), *Numerical Simulation of Rock Failure and Associated Seismicity*, Int. J. Rock Mech. Min. Sci. *34*, 249–262.

TOI, Y., and CHE, J. S. (1994), *Computational Damage Mechanics Models for Brittle Microcracking Solids Based on Mesoscopic Simulation*, Eng. Fracture Mech. *48*, 483–498.

TOI, Y., and KIYOSUE, T. (1995), *Damage Mechanics Models for Brittle Micro-cracking Solids Based on Three-dimensional Mesoscopic Simulation*, Eng. Fracture Mech. *50*, 11–27.

YIN, X. C., CHEN, X. Z., SONG, Z. P., and YIN, C. (1995), *A New Approach to Earthquake Prediction: The Load/Unload Response Ration (LURR) theory*, Pure appl. geophys. *145*, 701–715.

YIN, X. C., WANG, Y. C., PENG, K. Y., BAI, Y. L., WANG, H. T., YIN, X. F. (2000), *Development of a New Approach to Earthquake Prediction: Load/Unload Response Ratio (LURR) Theory*, Pure appl. geophys. *157*, 2365–2383.

(Received July 31, 1999, revised February 20, 2000, accepted April 28, 2000)